RSC Advances

ROYAL SOCIETY OF CHEMISTRY

www.rsc.org/advances

Cite this: DOI: 10.1039/c0xx00000x

www.rsc.org/xxxxxx

ARTICLE TYPE

Facile Synthesis and Gas-sensing Performance of Sr- or Fe-doped In_2O_3 Hollow Sub-microspheres

Xiaoping Shen[a,*], Lijun Guo[a], Guoxing Zhu[a], Chunyan Xi[a], Zhenyuan Ji[a] and Hu Zhou[b]

Received (in XXX, XXX) Xth XXXXXXXXX 20XX, Accepted Xth XXXXXXXXX 20XX

DOI: 10.1039/b000000x

Sr- or Fe-doped In_2O_3 hollow sub-microspheres were successfully fabricated without the assistance of any additives or templates. The obtained hollow In_2O_3 sub-microspheres show relatively uniform size and band gap of ~3.1 eV. Benefited from the hollow microstructure and doping effect, the doped In_2O_3 sub-microspheres show excellent gas sensing performance towards a series of organic solvents. For 100 ppm of formaldehyde, the Sr- and Fe-doped In_2O_3 sensors demonstrate sensing responses of 9.4 and 5.5, respectively. These values are much higher than previously reported In_2O_3-based gas sensors. Interestingly, Fe-doped In_2O_3 shows relatively higher sensing response to propanol than that of Sr-doped In_2O_3, although towards formaldehyde, ethanol, acetone and heptane, Sr-doped In_2O_3 shows relatively higher sensing responses. This investigation therefore indicates that doped In_2O_3 hollow microstructure could be an effective platform for sensing hazardous indoor formaldehyde gas, and that sensing selectivity could be improved by doping effect.

Introduction

Gas sensors, which are usually employed to detect various toxic and dangerous gases, to discriminate odor, or to monitor ambient gas atmosphere changes, have gained popularity because of their large requirement in the above listed fields and systems.[1-3] Among various gas sensors, metal oxide-based semiconductor gas sensors are especially attractive for solid-state detecting devices due to their high sensitivity, low cost, nontoxic, and high stability.[5-8] The basic detection principle of semiconductor gas sensors is the resistance change of sensing materials with gas adsorption.[4] Thus, the sensing material is crucial to the gas sensing performance.

For improving sensing properties of oxide-based sensors, one important route is to finely tune the shape and size of sensing materials through various chemical/physical methods.[9-12] Small micro-/nanoscale objects with high surface-to-volume ratio can provide more adsorption sites for sensing reaction, and thus induce higher capability to detect chemical and biological species. Among them, hollow micro-/nanospheres are the best candidate for gas sensing application, as gas diffusion in sensing materials is often an important factor that limits the overall performance, while making sensing materials into hollow micro-/nanospheres is expected to greatly facilitate the gas diffusion and to provide more adsorption sites for sensing reaction, thus ultimately to improve the sensing performances.[13] Up to date, many hollow oxide micro-/nanostructures have been prepared and investigated as gas sensing materials.[14-17] For example, Sun *et al* has demonstrated a hierarchical hollow structure composed of Fe_2O_3/NiO, which shows a sensing response of 18.7 to 100 ppm toluene.[18] With the assistance of CTAB, Sui *et al* prepared Cu_2O hollow structures, which show enhanced gas sensing property towards ethanol.[19]

For semiconducting oxides used as gas sensing materials, we are especially interested in In_2O_3, which is well known to be a typical *n*-type semiconductor.[20-22] Due to oxygen vacancy, it is usually in a non-stoichiometric form[23] and thus has been extensively applied in surface-related fields such as optoelectronic device, gas sensors, and so forth.[24] Zhang and co-workers[25] have demonstrated a single In_2O_3 nanowire transistor to work as a chemical sensor for detecting of NO_2 and NH_3 at room temperature. Recently, from gas-liquid chemical deposition-synthesized In_2S_3 nanoparticles, In_2O_3 nanoparticles are prepared by an following annealing route, which show excellent gas sensing performances for acetone detection.[26] Based on In_2O_3 truncated octahedron, Hu *et al* fabricated a gas sensor for detecting formaldehyde.[27]

Besides pure In_2O_3 materials, In_2O_3-based composites through doping or loading by a secondary component are also investigated for gas sensing.[28-39] Generally, the doped or loaded components can act as catalysts or sensitizers for sensing reaction, thus providing improved sensing performances. For example, Pd-loaded In_2O_3 nanowire-like networks exhibit superior sensitivity with short response and recovery times for detection of NO_2 gas.[35] Zhang *et al* prepared RE (RE = La, Er, Yb) doped In_2O_3 hollow spheres, which show enhanced alcohol-sensing properties. They attributed the enhancement effect to the change of lattice defect and chemisorbed oxygen.[31] Zn-doped In_2O_3 flower-like structures were also prepared, which exhibit a higher response to NO_2 .[38]

Despite the above considerable efforts devoted to In_2O_3-based gas sensors, there is vast space for further exploits. The sensing

properties of the obtained gas sensors are still poor and cannot fully fulfill the actual requirement. Herein, we present a simple synthesis route for hollow In_2O_3 sub-microspheres doped by Sr or Fe. The obtained hollow In_2O_3 sub-microspheres have a size of ~600 nm. Interestingly, the hollow sphere shell is further composed of tiny nanoparticles. Benefited from the unique microstructure and the doping effect, the as-prepared Sr-doped and Fe-doped In_2O_3 products show excellent gas sensing performance towards a series of typical organic solvents including formaldehyde, propanol, and so on.

Experimental Section

Chemicals

All chemical reagents employed in our study are analytical grade and used without further purification. All are purchased from Sinopharm Chemical Reagent Co., Ltd. Indium acetylacetonate [$In(acac)_3$] was synthesized according to the literature method.[40]

Synthesis of doped In_2O_3 hollow spheres

In a typical procedure, 0.1 g of $In(acac)_3$ and 5.5 mg of $Sr(NO_3)_2$ (with mole ratio of Sr : In = 1: 10) was dispersed in 20 mL of ethylenediamine with strongly stirring. The obtained mixture was poured into a Teflon-lined stainless steel autoclave, which was heated to 180 ^oC and maintained at that temperature for 12 h. The obtained precipitate (Sr-doped In_2O_3 product) was then separated by centrifugation, washed with distilled water and ethanol for several times, and dried in vacuum at 40 ^oC for 6 h. With similar route, Fe-doped In_2O_3 product was also prepared with 0.1 g of $In(acac)_3$ and 10 mg of $Fe(NO_3)_3 \cdot 9H_2O$ (with mole ratio of Fe : In = 1: 10).

Characterization and measurements

The composition, morphology, and size of the samples were examined by scanning electron microscopy (SEM, JSM-6480) and transmission electron microscopy (TEM, JEOL-2100). Elemental mapping was also conducted on the HRTEM microscopy. The crystal phase of the as-synthesized products was characterized by X-ray diffraction (XRD, Shimadzu XRD-6000) with Cu Kα radiation (λ = 1.5406 Å) at a scanning rate of $4^o \cdot min^{-1}$. The X-ray tubes were operated with electric current of 30 mA and voltage of 40 kV. Optical diffuse reflectance spectra were collected at room temperature with a UV-2450 UV-vis spectrophotometer. $BaSO_4$ powder was used as a standard (100% reflectance). X-ray photoelectron spectroscopy (XPS) was performed with an X-ray photoelectron spectrometer (Thermo ESCALAB 250) using monochromatic Al Ka (1486.6 eV) X-ray radiation.

Fabrication and measurement of gas sensor

The gas-sensing properties were measured using a WS-30A gas sensor measurement system (Weisheng Instruments Co., Zhengzhou, China). The gas sensor was fabricated as our previous reports.[41] Typically, a certain amount of the doped sample was firstly mixed with terpineol binder to form slurry through milling, and then pasted on to the ceramic tube, which was then assembled into the tested system through four platinum wires connected on it. The sample loaded on the ceramic tube was determined to be ~1 mg. The working temperature of the sensor is controlled by adjusting the heating voltage ($V_{heating}$) across a resistor inside the ceramic tube. A reference resistor is put in series with the sensor to form a complete measurement circuit. In the test process, a working voltage ($V_{working}$) was applied. By monitoring the voltage (V_{output}) across the reference resistor, the response of the sensor in a test gas could be measured. In our test, the reference resistor is 200 kΩ and the $V_{working}$ is 5 V. Gas-sensing measurements were carried out at the working temperature of 200 ºC with 25-35% relative humidity. The sensing response (R) was defined as the ratio of R_{air}/R_{gas}, which are the resistance in air and tested gas, respectively.

Results and discussion

The doped In_2O_3 samples were prepared by a simple solvothermal process with $In(acac)_3$ as the indium source and ethylenediamine as the solvent. $Sr(NO_3)_2$ and $Fe(NO_3)_3$ were selected as dopant agents, respectively. The as-formed doped samples were firstly detected by XRD. As shown in Figure 1, the XRD patterns can be readily indexed to cubic structure In_2O_3 with lattice constants a = 10.14 Å (JCPDS card No. 65-3170). The main peaks at 22.5º, 30.8º, 35.6º, 51.1º, and 60.9º correspond to the (211), (222), (400), (440), and (622) lattice planes of cubic In_2O_3, respectively. The relatively wide peak suggests the smaller size of In_2O_3 crystalline. It should be noted that no peaks corresponding to SrO or Fe_2O_3, Fe_3O_4 were detected in the XRD patterns, suggesting no separated oxide phase was formed in the product.

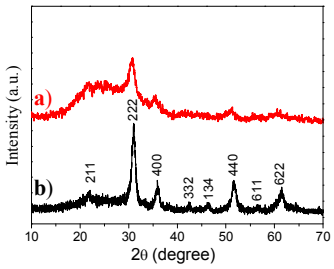

Fig. 1 X-ray diffraction patterns of the doped In_2O_3 products, which can be indexed to the standard pattern of In_2O_3 with JCPDS No. 64-3170. a) Sr-doped In_2O_3 and b) Fe-doped In_2O_3.

The elemental composition of the doped In_2O_3 products was firstly detected by EDS analysis, which was conducted on a SEM (Fig. SI-1, see Supporting Information). Both of the two samples show the elements of oxygen, carbon, indium, and platinum. Carbon and platinum come from the conductive binder and surface conductive layer for SEM sample preparation. In the sample of Sr-doped In_2O_3, Sr is detected indicating Sr is doped into the sample. Similarly, the peak corresponding to Fe is found in the spectrum of Fe-doped In_2O_3 product. These results show that Fe or Sr exists in the samples.

The morphology and size of the as-prepared In_2O_3 products were then characterized by SEM and TEM. SEM images of the Sr-doped In_2O_3 product are shown in Figure 2a-b. The Sr-doped In_2O_3 product is composed of spherical structures. The diameter is in the range of 400-800 nm. Interestingly, some of the sub-microspheres demonstrate broken structure, revealing their hollow interior. Careful observation of the magnified SEM image

found that the shell of the hollow spheres is actually formed by the stacking of tiny nanoparticles. This unique hollow structure is further revealed by TEM analysis. Figure 2c shows the corresponding TEM image. The different contrast between the interior and the surface further confirms the hollow structures. It can be clearly seen that the hollow spherical shell has a thickness of 60-100 nm.

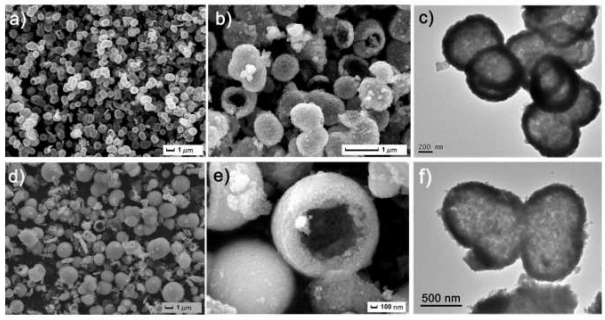

Fig. 2 SEM and TEM images of a, b, c) Sr-doped and d, e, f) Fe-doped In_2O_3 hollow sub-microspheres.

Fe-doped In_2O_3 show similar hollow sub-microsphere structure, although its uniformity is not as good as that of Sr-doped In_2O_3. The Fe-doped In_2O_3 product has bigger size of 800-1500 nm, suggesting the strong influence of the dopant on the final morphology (Figure 2d-f). The formation mechanism of hollow spheres is not clear at present stage. Probably, it would relate to the generated gas bubbles during the reaction, which act as template for the formation of the hollow spheres. It should be noted that without the dopant agents, $Sr(NO_3)_2$ or $Fe(NO_3)_3$, the obtained pure phase In_2O_3 also shows spherical-like shape, but demonstrating porous structure feature (Fig. SI-2, see Supporting Information). We also tried to prepare Bi-doped In_2O_3 product, as confirmed by XRD, a mixture of metallic Bi and In_2O_3 instead of Bi-doped In_2O_3 was obtained, although the product also shows hollow spherical structure (Fig. SI-3, see Supporting Information). The obtained Sr or Fe-doped In_2O_3 hollow structure will inevitably increase the surface area and provide a suitable channel for substance transport, thus would show improved gas sensing properties.

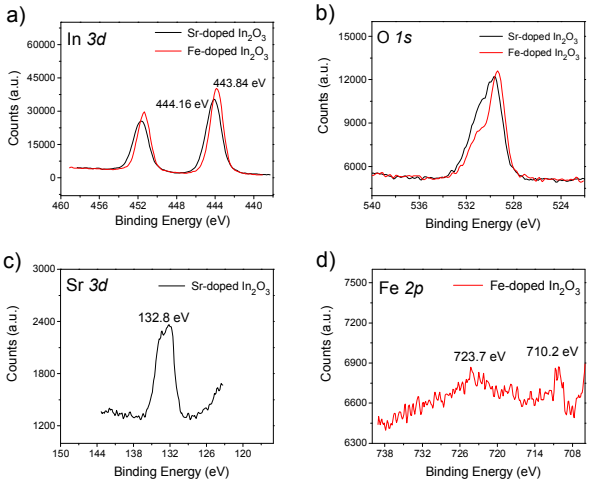

Fig. 3 XPS spectra of the doped In_2O_3 products. a) In 3d region, b) O 1s region, c) Sr 3d region, and d) Fe 2p region.

The element compositions of the Sr- or Fe-doped In_2O_3 product were then further studied by XPS analysis as shown in Figure 3. The XPS spectra show that both of the obtained products are composed of indium and oxygen (Figure 3a and b). Figure 3c and d show the high resolution spectra of Sr and Fe elements, respectively. The peak at 132.8 eV can be attributed to Sr^{2+}. The binding energies of Fe 2p 3/2 and Fe 2p 1/2 are centered at 710.2 and 723.7 eV, respectively, indicating the existence of Fe^{3+} in the products.

Figure 3a gives the characteristic high resolution spectra of In 3d with spin-orbit split for In 3d 5/2 and In 3d 3/2 of In^{3+}. The peaks of In 3d5/2 for Sr-doped In_2O_3 (444.16 eV) is a little bigger than that of pure In_2O_3 (444.09 eV)[31] and Fe-doped In_2O_3 (443.84 eV). This would relate to the charge density difference for different metal ions. The ion radius of Sr^{2+}, Fe^{3+}, In^{3+} are 144, 64, and 80 pm, respectively. The higher charge density Fe^{3+} ions will withdraw the electrons from indium, so the screening effect of electrons would decrease for indium. Thus, the corresponding binding energies of In^{3+} decrease.[42, 43] This result implies that Sr^{2+}, Fe^{3+} ions were doped into the In_2O_3 lattice, inducing an electronic interaction. In addition, elemental mapping images (Figure 4) show that the elements of In, O, and Sr or Fe are uniformly distributed in the whole hollow spheres, confirming the highly uniform distribution of Sr and Fe elements in the products.

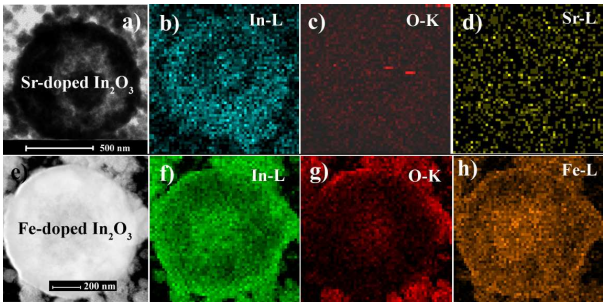

Fig. 4 Elemental mapping images of a-d) Sr-doped In_2O_3 and e-h) Fe-doped In_2O_3.

The optical absorption properties of the two doped samples were then tested by using ultraviolet-diffuse reflectance spectroscopy (Figure 5a). From the obtained spectra, the obvious absorption band edge was shown at about ~500 nm for both the products. Optical band gap energy can be estimated by the well-known formula, $(\alpha h\nu)^n = B(h\nu - E_g)$, where α is the absorption coefficient, $h\nu$ is the photon energy, B is a constant characteristic of the material, E_g is the band gap, and n is either 1/2 for an indirect transition or 2 for a direct transition. The band gaps of the doped In_2O_3 products with a direct transition were evaluated. Figure 5b depicts the corresponding Kubelka-Munk transformed reflectance spectra with $n = 2$, which show 3.15 eV for Sr-doped In_2O_3 and 3.06 eV for Fe-doped In_2O_3. These values are comparable to the reported values, for example, 3.7 eV for bulk In_2O_3,[44] 3.2-3.8 eV for In_2O_3 films.[45] The relatively small band gap would originate from the unique hollow structure and/or the presence of the dopants.

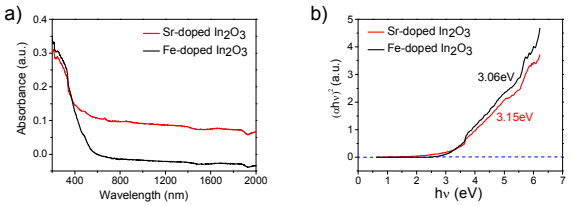

Fig. 5 a) UV-vis diffuse reflectance spectra recorded in the reflectance mode of the doped In_2O_3 products. b) The corresponding $(\alpha h\nu)^2$ *vs.* hν curves, from which the band gap energy is estimated.

Owing to the bigger surface area, rich accessible surface active sites, and excellent gas transport channel, hollow structure is highly preferred for sensing materials. Thus, it is believed that the doped In_2O_3 hollow sub-microspheres would own improved gas sensing properties. A toxic gas, formaldehyde, which is used predominantly as a chemical intermediate and is often released from various consumer products such as building materials and home furnishings, was firstly selected as a model test gas for the sensing performance investigation.

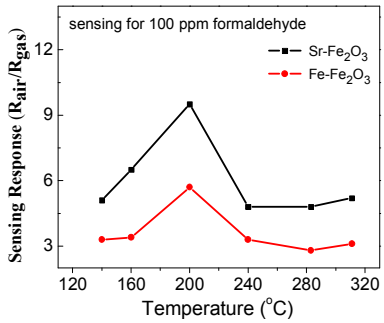

Fig. 6 Sensing responses of the doped In_2O_3 products to 100 ppm of formaldehyde at different temperatures.

It is known that the sensing response is greatly influenced by operating temperature, because the analyte adsorption-desorption kinetics is temperature dependent. Thus we measured the sensing performances of the doped In_2O_3 products at different operating temperatures towards 100 ppm of formaldehyde (Figure 6). It was found that the sensing responses increase at relatively lower temperature and then decrease at higher working temperature. Both of the optimum operating temperatures for the doped In_2O_3 products to formaldehyde are 200 °C. The temperature-dependence of the sensing response is reasonable, since the gas diffusion behavior, and the reaction kinetics between analyte gas and surface-adsorbed oxygen are all temperature dependent.

The sensing responses with operating temperature of 200 °C towards formaldehyde of the doped In_2O_3 sensors are displayed in Figure 7, which records nine successive sensing cycles, corresponding to nine different concentrations in the range of 5-1000 ppm. As shown in Figure 7a, the conductance of the doped sensors undergoes a drastic rise once the injection of formaldehyde to the test chamber and drops to its baseline if the sensors are further exposed to fresh air, revealing the excellent sensing response. The sensing response (R_{air}/R_{gas}) values increase with the increasing of formaldehyde concentration in the range of 5-1000 ppm. After nine successive sensing cycles, the conductance can resume to its baseline, suggesting the good reproducibility.

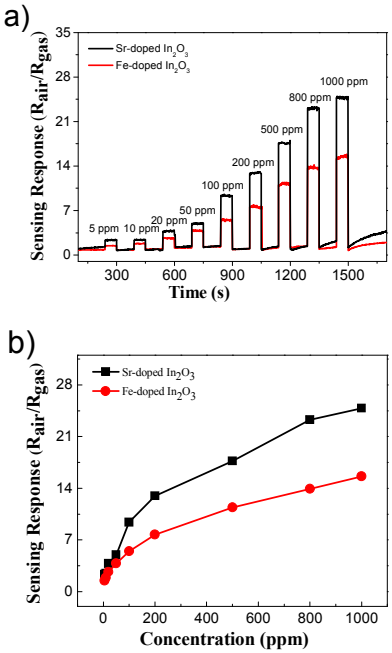

Fig. 7 a) Real-time sensing responses and b) plots of sensing response *vs.* concentration towards formaldehyde of the sensors made from the doped In_2O_3 products with operating temperature of 200 °C.

With equal concentration of formaldehyde, the response magnitude of the Sr-doped In_2O_3 is higher than that of the Fe-doped In_2O_3. Towards 100 ppm of formaldehyde, the Fe-doped In_2O_3 show sensing response of 5.5. In contrast, that of the Sr-doped In_2O_3 is 9.4. The sensing detection limit can be down to 5 ppm. For 5 ppm of formaldehyde, the sensing response of the Sr-doped In_2O_3 is 2.4, suggesting the excellent sensing properties.

The curves of sensing response as a function of formaldehyde concentration are shown in Figure 7b. The response values increase with the increasing formaldehyde concentration. The sensors show a near linear response to formaldehyde concentration in the range of 5-200 ppm, while beyond that, the response to formaldehyde gradually saturates. This may be attributed to the insufficiency of negatively charged oxygen ions on the sensor which cannot oxidize all the analyte gases on the sensor surface and/or the full covering of gas molecules on the sensor.[46]

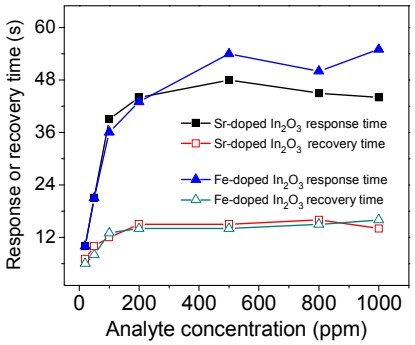

Fig. 8 The response and recovery times of Sr-doped In_2O_3 and Fe-doped In_2O_3 sensors as a function of formaldehyde concentration.

Both of the doped sensors have a relatively quick sensing response and recovery times, which are defined as the time to reach 90% of the final equilibrium value. As shown in Figure 8, the response and recovery times of the two sensors are formaldehyde concentration dependent. It seems that the two sensors show similar response and recovery behaviors towards formaldehyde. With formaldehyde concentration smaller than 200 ppm, the response and recovery times increased with the increasing concentration. While with the concentration bigger than 200 ppm, the response and recovery times almost maintain at certain values with response time of ~50 s and recovery time of ~15 s. It should be noted that the recorded response times in our case contain three parts of time, the evaporation time of formaldehyde on the evaporator, the diffusion time of formaldehyde from the evaporator to the sensor surface, the reaction time between formaldehyde and surface-adsorbed oxygen. Thus, the response time (~50 s) is much longer than that of recovery time (~15 s).

It is generally accepted that gas sensing mechanism of oxides comes from the fact that the electric conductivity of a semiconductor depends on the surface adsorption and desorption of oxygen ion species. As a typical *n*-type semiconductor, the surface of In_2O_3 is readily covered with negatively charged chemisorbed oxygen ions, such as O_2^-, O^{2-}, O^-. These chemisorbed oxygen ions cause the generation of electron depletion layers on its surface according to the follow reactions:[47]

$$O_2\ (ads) + e^- \leftrightarrow O_2^-$$
$$O_2^-\ (ads) + e^- \leftrightarrow 2O^- \text{ or } O_2^{2-}$$
$$O^-\ (ads) + e^- \leftrightarrow O^{2-}$$

When reduction gas molecules were involved in the test chamber, their reaction with these chemisorbed oxygen ions will again release the anchoring electrons into the In_2O_3 phase. This reaction causes the conductance increase and induces the gas sensing.

Table 1. Sensing properties of In_2O_3 based sensors towards formaldehyde.

Samples	Operating temperature	Gas concentration (ppm)	Response	Limit of detection (ppm)	Refs
Cubic In_2O_3 nanoparticles	200	100	~1.8	100	48
Hexagonal In_2O_3 nanoparticles	200	100	~1.1	100	48
SnO_2/In_2O_3 nanofibers	280	50	~2.5	/	49
In_2O_3 hollow microspheres	/	80	~4.5-11	10	50
In_2O_3-SnO_2 nanotoasts	300	50	~2.1-10	/	51
Sr-doped In_2O_3	200	100	9.4	5	This work
Fe-doped In_2O_3	200	100	5.5	5	This work

For comparison, the sensing responses to formaldehyde obtained here are compared with those reported previously. The result is shown in Table 1. It is obvious that the doped In_2O_3 sensors prepared in this work exhibit relatively higher sensing responses and lower detection limit to formaldehyde. It is proposed that the relatively better gas sensing properties would originate from the unique microstructure and/or the effective doping. The hollow structure stacked by tiny nanoparticles endows the bigger surface area, which is highly preferred for oxygen adsorption and the followed gas sensing process. In addition, the dopant element could play a catalytic role for the sensing reaction.

The gas sensing performance of the doped In_2O_3 products towards other several organic solvents was also investigated. The tested substances include acetone, heptane, propanol, ethanol, and toluene, which are also widely used as important industrial raw materials. Highly sensitive detection of them is also urgently needed because of their flammability and toxicity. The corresponding sensing responses to 5 and 100 ppm concentrations of them are shown in Figure 9. For the two doped products, the Sr-doped In_2O_3 shows higher sensing response than Fe-doped In_2O_3 towards acetone, heptane, formaldehyde, and ethanol. While, for propanol, the Fe-doped In_2O_3 shows relatively higher sensing response. This demonstrates that doping of Fe in In_2O_3 will highly improve their sensing selectivity for propanol and gives an avenue for design of sensors with high sensing selectivity. While, at present stage, it is still difficult to in depth understand the detailed mechanism of gas sensors with different selectivity since the gas sensing behavior is influenced by several factors such as analyte diffusion behavior, analyte adsorption on the sensing materials, the surface catalytic reaction, and so on. The different sensing selectivity of the two gas sensors would attribute to the different adsorption and catalytic properties towards different analytes endowed by the incorporation of dopant ions.

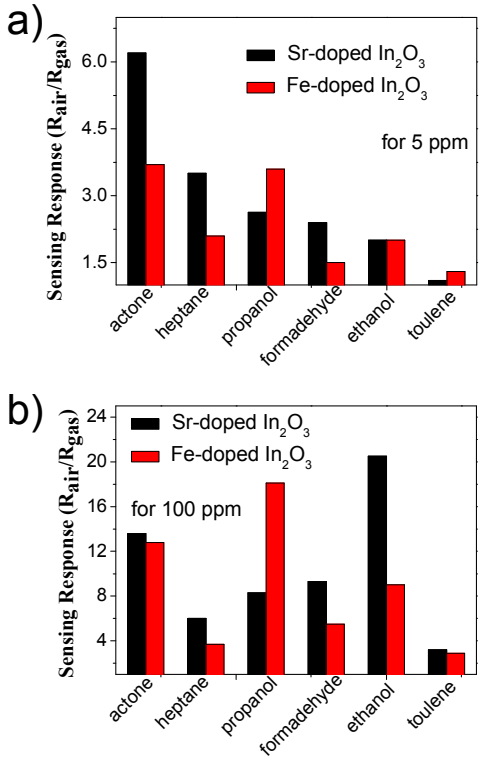

Fig. 9 Sensing responses of the doped In_2O_3 sensors towards a) 5 ppm and b) 100 ppm of acetone, heptane, propanol, formaldehyde, ethanol, and toluene.

Conclusions

In summary, with a simple solvothermal route, Sr- or Fe-doped In_2O_3 hollow sub-microspheres have been successfully synthesized without any additives. The obtained hollow products are further composed of many tiny nanoparticles. Gas sensors based on the doped In_2O_3 hollow sub-microspheres are fabricated and investigated with HCHO as the main probe gas. It is found that Sr-doped In_2O_3 shows an excellent sensing performance towards to formaldehyde. Towards 100 ppm of HCHO, the sensing response of Sr-doped In_2O_3 is as high as 9.6. The excellent sensing property could be ascribed to their unique microstructure and the doping effect. This result highlights the potential applications of the doped In_2O_3 hollow submicrospheres in development of advanced formaldehyde-sensing materials.

Acknowledgements

The authors are grateful for financial support from the National Natural Science Foundation of China (Nos. 51272094 and 51102117) and the Specialized Research Fund for the Doctoral Program of Higher Education of China (No. 20123227110018).

Notes and references

[a] *School of Chemistry and Chemical Engineering, Jiangsu University, Zhenjiang 212013, P. R. China*
[b] *School of Materials Science and Engineering, Jiangsu University, Zhenjiang 212013, P. R. China*
**Corresponding author. Tel/Fax: +86-511-88791800.*
E-mail address: xiaopingshen@163.com.

† Electronic Supplementary Information (ESI) available: [EDS spectrum of Sr- or Fe-doped In_2O_3, SEM image and XRD pattern of Bi-In_2O_3 product]. See DOI: 10.1039/b000000x/

1. P. R. Chung, C. T. Tzeng, M. T. Ke, C. Y. Lee, *Sensors*, 2013, **13**, 4468.
2. C. D. Natale, R. Paolesse, E. Martinelli, R. Capuano, *Analyt. Chim. Acta*, 2014, **824**, 1.
3. S. Das, V. Jayaraman, *Prog. Mater. Sci.*, 2014, **66**, 112.
4. N. Ramgir, N. Datta, M. Kaur, S. Kailasaganapathi, A. K. Debnath, D. K. Aswal, S. K. Gupta, *Colloid Surf. A-Phys. Eng. Aspects*, 2013, **439**, 101.
5. M. M. Arafat, B. Dinan, S. A. Akbar, A. S. M. A. Haseeb, *Sensors*, 2012, **12**, 7207.
6. H. S. Gu, Z. Wang, Y. M. Hu, *Sensors*, 2012, **12**, 5517.
7. G. W. Ho, *Sci. Adv. Mater.*, 2011, **3**, 150.
8. G. Korotcenkov, B. K. Cho, *Sensor Actuat. B-Chem.*, 2014, **196**, 80.
9. S. Trocino, P. Frontera, A. Donato, C. Busacca, L. A. Scarpino, P. Antonucci, G. Neri, *Mater. Chem. Phys.*, 2014, **147**, 35.
10. N. Kilinc, O. Cakmak, A. Kosemen, E. Ermek, S. Ozturk, Y. Yerli, Z. Z. Ozturk, H. Urey, *Sensor. Actuat. B-Chem.*, 2014 , **202**, 357.
11. N. Rajesh, J. C. Kannan, S. G. Leonardi, G. Neri, T. Krishnakumar, *J. Alloy. Compd.*, 2014, **607**, 54.
12. L. Li, M. M. Liu, S. J. He, W. Chen, *Anal. Chem.*, 2014, **86**, 7996.
13. J. S. Cui, J. B. Sun, X. Liu, J. W. Li, X. Z. Ma, T. T. Chen, *Appl. Surf. Sci.*, 2014, **308**, 17.
14. S. Q. Liu, Y. X. Li, M. J. Xie, X. F. Guo, W. J. Ji, W. P. Ding, Y. Chen, *J. Nanosci. Nanotechno.*, 2010, **10**, 6725.
15. J. H. Lee, *Sensor. Actuat. B-Chem.*, 2009, **140**, 319.
16. G. L. Li, H. Mohwald, D. G. Shchukin, *Chem. Soc. Rev.*, 2013, **42**, 3628.
17. Y. S. Li, J. L. Shi, *Adv. Mater.*, 2014, **26**, 3176.
18. C. Wang, X. Y. Cheng, X. Zhou, P. Sun, X. L. Hu, K. Shimanoe, G. Y. Lu, N. Yamazoe, *ACS Appl. Mater. Interfaces*, 2014, **6**, 12031.
19. Y. M. Sui, Y. Zeng, L. L. Fu, W. T. Zheng, D. M. Li, B. B. Liu, B. Zou, *RSC Adv.*, 2013, **3**, 18651.
20. D. H. Zhang, C. Li, S. Han, X. L. Liu, T. Tang, W. Jin, C. W. Zhou, *Appl. Phys. Lett.*, 2003, **82**, 112.
21. A. Gurlo, M. Ivanovskaya, N. Bârsan, M. Schweizer-Berberich, U. Weimar, W. Göpel, A. Diéguez, *Sensor. Actuat. B-Chem.*, 1997, **44**, 327.
22. C. G. Granqvist, *Appl. Phys. A: Solids Surf.*, 1993, **57**, 19.
23. B. P. Bastakoti, H. Oveisi, C. C. Hu, K. C. W. Wu, N. Suzuki, K. Takai, Y. Kamachi, M. Imura, Y. Yamauchi, *Eur. J. Inorg. Chem.*, 2013, **2013**, 1109.
24. L. Zhao, W. B. Yue, Y. Ren, *Electrochim. Acta*, 2014, **116**, 31.
25. A. Shanmugasundaram, B. Ramireddy, P. Basak, S. V. Manorama, S. Srinath, *J. Phys. Chem. C*, 2014, **118**, 6909.
26. S. M. Wang, P. Wang, Z. F. Li, C. H. Xiao, B. X. Xiao, R. Zhao, T. Y. Yang, M. Z. Zhang, *New J. Chem.*, 2014, **38**, 4879.
27. W. Yang, P. Wan, X. D. Zhou, J. M. Hu, Y. F. Guan, L. Feng, *Sensor. Actuat. B-Chem.*, 2014, **201**, 228.
28. Y. R. Wang, B. Liu, D. P. Cai, H. Li, Y. Liu, D. D. Wang, L. L. Wang, Q. H. Li, T. H. Wang, *Sensor. Actuat. B-Chem.*, 2014, **201**, 351.
29. W. L. Zang, Y. X. Nie, D. Zhu, P. Deng, L. L. Xing, X. Y. Xue, *J. Phys. Chem. C*, 2014, **118**, 9209.
30. J. Zhao, T. L. Yang, Y. P. Liu, Z. Y. Wang, X. W. Li, Y. F. Sun, Y. Du, Y. C. Li, G. Y. Lu, *Sensor. Actuat. B-Chem.*, 2014, **191**, 806.
31. T. Zhang, F. B. Gu, D. M. Han, Z. H. Wang, G. S. Guo, *Sensor. Actuat. B-Chem.*, 2013, **177**, 1180.
32. N. G. Pramodn, S. N. Pandey, *Ceram. Int.*, 2014, **40**, 3461.
33. X. Chi, C. B. Liu, L. Liu, S. C. Li, H. Y. Li, X. B. Zhang, X. Q. Bo, H. Shan, *Mater. Sci. Semicon. Proc.*, 2014, **18**, 160.
34. H. F. Yang, X. Zhang, J. F. Li, W. T. Li, G. C. Xi, Y. Yan, H. Bai, *Microp. Mesop. Mater.*, 2014, **200**, 140.
35. M. Q. Huang, Z. D. Cui, X. J. Yang, S. L. Zhu, Z. Y. Li, Y. Q. Liang, *RSC Adv.*, 2015, **5**, 30038.
36. L. Y. Yao, K. Kan, Y. F. Lin, J. B. Song, J. C. Wang, J. Gao, P. K. Shen, L. Li, K. Y. Shi, *RSC Adv.*, 2015, **5**, 15515.
37. Y. M. Nikolaenko, Y. E. Kuzovlev, Y. V. Medvedev, N. I. Mezin, C. Fasel, A. Gurlo, L. Schlicker, T. J. M. Bayer, Y. A. Genenko, *J. Appl. Phys.*, 2014, **116**, 043704.
38. P. Li, H. Q. Fan, Y. Cai, M. M. Xu, C. B. Long, M. M. Li, S. H. Lei, X. W. Zou, *RSC Adv.*, 2015, **4**, 15161.
39. P. Li, H. Q. Fan, Y. Cai, M. M. Xu, *CrystEngComm*, 2014, **16**, 2715.
40. G. T. Morgan, H. D. K. Drew, *J. Chem. Soc.*,1921, **119**, 1058.
41. G. X. Zhu, Y. J. Liu, C. Y. Xi, C. L. Bao, H. Xu, X. P. Shen, X. L. Zhu, *CrystEngComm*, 2013, **15**, 9189.
42. T. Chen, Q. J. Liu, Z. L. Zhou, Y. D. Wang, *Sensor. Actuat. B-Chem.*, 2008, **131**, 301.
43. L. Xu, H. W. Song, B. Dong, Y. Wang, J. S. Chen, X. Bai, *Inorg. Chem.*, 2010, **49**, 10590.
44. D. P. Dutta, V. Sudarsan, P. Srinivasu, A. Vinu, A.K. Tyagi, *J. Phys. Chem. C*, 2008, **112**, 6781.
45. A. K. Bal, A. Singh, R. K. Bedi, *Physica B*, 2010, **405**, 3124.
46. G. X. Zhu, C. Y. Xi, H. Xu, D. Zheng, Y. J. Liu, X. Xu, X. P. Shen, *RSC Adv.*, 2012, **2**, 4236.
47. H. Kim, J. Lee, *Sensor. Actuat. B-Chem.*, 2014, **192**, 607.
48. X. Q. Wang, M. F. Zhang, J. Y. Liu, T. Luo, Y. T. Qian, *Sensor. Actuat. B-Chem.*, 2009, **137**, 103.
49. W. Zheng, X. F. Lu, W. Wang, B. Dong, H. N. Zhang, Z. J. Wang, X. R. Xu, C. Wang, *J. Am. Ceram. Soc*, 2010, **93**, 15.
50. B. X. Li, Y. Xie, M. Jing, G. X. Rong, Y. C. Tang, G. Z. Zhang, *Langmuir*, 2006, **22**, 9380.
51. D. W. Chu , Y. P. Zeng, D. L. Jiang, Y. Masuda, *Sensor. Actuat. B-Chem.*, 2009, **137**, 630.

TOC

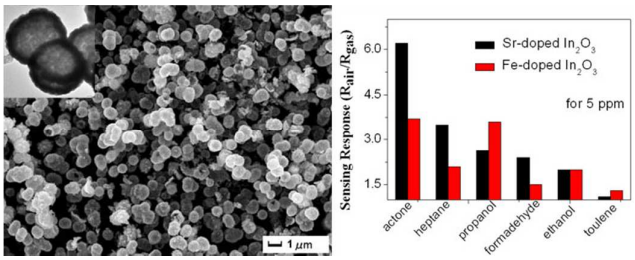

Sr- or Fe-doped In_2O_3 hollow sub-microspheres were successfully fabricated, which show excellent gas sensing performance towards a series of organic solvents.